Chapter 5

Application of Finite Element Analysis in Multiscale Metal Forming Process

Zhengyi Jiang and Haibo Xie

Additional information is available at the end of the chapter

http://dx.doi.org/10.5772/intechopen.71880

Abstract

The application of finite element analysis has been presented in multiscale metal forming process. A 3D finite element method (FEM) has first been proposed to analyze the deformation mechanism of thin strip cold rolling with the consideration of friction variation in deformation zone. The crystal plasticity finite element method (CPFEM) is applied on the simulation of surface asperity flattening in the uniaxial planar compressing process. 3D Voronoi tessellation and frictional modeling have been applied in microforming processes. All simulation results from the proposed modeling have been validated by the related experimental results.

Keywords: multiscale, metal forming, FEM, friction variation, Voronoi tessellation, size effect

1. Introduction

Process modeling for the investigation and understanding of deformation mechanics has become a major concern in research, and the application of the finite element method (FEM) has been tremendously increased, particularly in the modeling of forming processes. There are many research studies on the principles and fundamentals of the simulation of metal forming, but only a few studies describe the application of FEM to the analysis and simulation of multiscale forming processes. The main objective of this chapter is to present the applications of FEM in metal forming analysis from macroscale to microscale.

Friction at the strip-roll interface is an important consideration in the metal-forming process. Traditionally, the frictional force is assumed to be proportional to the normal force, and the friction coefficient keeps the same in the roll bite. This assumption conflicts with the research

results where the friction is changeable in the roll bite [1], and the rolling pressure and model control accuracy will be influenced significantly. The deformation mechanics of thin foil [2] and the foil rolling with constant friction during cold rolling [3] have been investigated. The finite element method has been proposed in special-shaped strip rolling [4–6], particularly with variable friction models [5, 6]. Considering modeling accuracy, a friction variation model should be introduced in the cold rolling simulation of thin strip.

The application of crystal plasticity finite element method (CPFEM) has been introduced in the simulation of surface asperity flattening in cold quasistatic uniaxial planar compression process. Rate-dependent crystal plasticity constitutive models have been established on the basis of experimental conditions [7], and the influences of the reduction and strain rate on the surface roughness are investigated using the 3D crystal plasticity finite element method [8]. The experimental results are also employed in the 3D CPFEM model and compared with the simulation results.

Microforming differs from the conventional forming technology in terms of materials, processes, tools, and machines and equipment due to the miniaturization nature of the whole microforming system [9]. It is impossible to scale down all parameters in the microforming process according to the theory of similarity due to the existence of size effects in microforming processes. A number of unexpected problems in key aspects of mechanical behavior, tribology, and scatter of material behavior are encountered [10, 11]. Challenges remain in the high efficiency manufacturing of high-quality microproducts due to the common problem of microscale size effects [9, 11], complexity of processes for making microproducts, and the ever increasing requirement to improve product quality and performance.

In Section 4, novel material model with grained heterogeneity in 3D Voronoi tessellation has been developed in the simulation of micro cross wedge rolling, springback analysis in micro flexible rolling and the micro V-bending processes considering grain boundary and generation process of grains in the workpiece [12–16]. The modified FE model in microforming has been applied with the consideration of size effects including material characterization, friction/contact characterization, and other size-related factors presented in Section 5. Open and closed lubricate pocket (OCLP) theory and size-dependent friction coefficient are proposed in micro deep drawing (MDD) and micro hydromechanical deep drawing (MHDD) [17–19]. Real microstructures and Voronoi structures are applied in microstructural models through the image-based modeling method [20, 21].

2. FEM analysis applied to thin strip rolling

The three-dimensional (3D) finite element method (FEM) has been used in the analysis of strip rolling, shape rolling, and slab rolling, and Jiang et al. [4–6, 22] used this finite element method to solve special-shaped strip rolling. This is a major drawback to producing accurate and reliable models for the cold rolling of thin strip due to the lack of well-defined friction boundary conditions. The 3D rigid plastic FEM has been proposed to solve the thin strip rolling considering friction variation in the deformation zone, and the comparison between the computed results and measured values has also been made.

http://dx.doi.org/10.5772/intechopen.71880

In the friction variation model, the friction varies along the contact length of the deformation zone. The frictional shear stress model is modified as [5]:

$$\tau_f = K_i \frac{m_1 \sigma_s}{\sqrt{3}} \left(\frac{2}{\pi} tan^{-1} \left\{ \frac{V_g}{k_i} \right\} \right) \quad (1)$$

where m_1 is the friction factor; σ_s yields stress; K_i is a coefficient of the friction shear stress changes with K_1 and K_2 for forward slip zone and backward slip zone, respectively; k_i is a positive constant with k_1 and k_2 for forward slip zone and backward slip zone, respectively; V_g is relative slip velocity between the strip and the roll and can be obtained by:

$$V_g = \sqrt{(v_x \, sec\beta - V_R)^2 + v_y{}^2} \quad (2)$$

where v_x and v_y are the velocity components in the x and y directions, respectively, β is the angular position of the node, V_R is the tangential velocity of the roll, and the distribution of these frictional shear stress models is shown in **Figure 1**.

As shown in **Figure 2**, a quarter of the strip was studied. Isoparametric hexahedral elements were applied with eight Gauss points throughout the deformed workpiece. The element number in x, y, and z directions are 10, 8, and 5, respectively, and totally there are 594 nodes and 400 elements.

From the simulation with low carbon steel, **Figures 3** and **4** show the effect of reduction on rolling pressure and spread of strip for different k_2 and constant k_1 = 0.1. k_2 influences the simulation results significantly where the rolling pressure increases with decreased k_2. When k_2 value is below 0.1, the rolling pressure calculation value is in agreement with the measured one. The spread calculation value for k_2 = 0.1 is also close to the measured one when the reduction is less than 43%. For k_2 = 0.1, the change of k_1 also has an effect on the simulation results, as shown in **Figures 5** and **6**. It can be seen that the calculated results are in good agreement with the measured values for k_1= 0.1. Therefore, the simulation results are close to measured values when k_1 and k_2 are less than 0.1.

The rolling of copper strip is simulated with work roll diameter 158.76 mm, width of strip 76.2 mm, rolling speed 0.16 m/s, and friction factor m_1 = 0.4. For case 1, $K_1 = K_2 = 1.0$ and $k_1 = k_2 = 0.1$

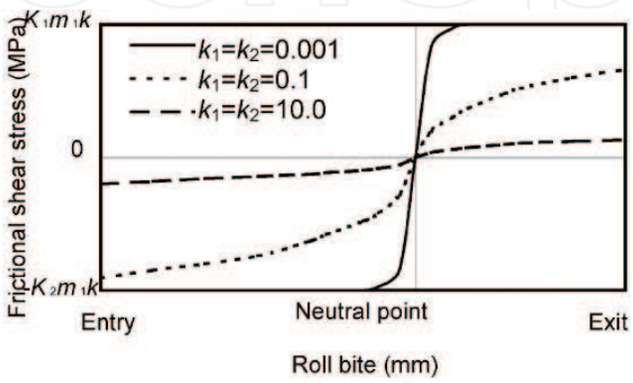

Figure 1. Frictional shear stress models.

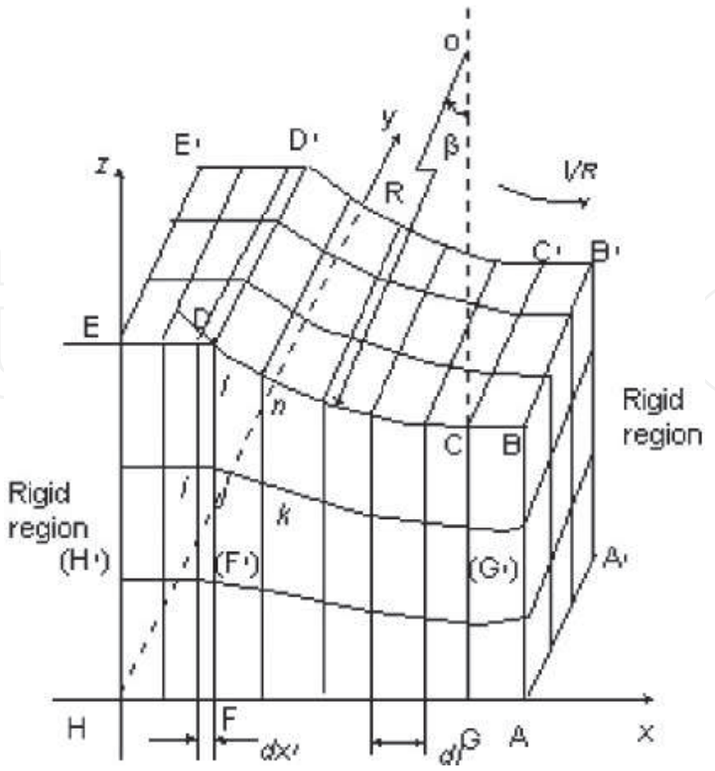

Figure 2. One-quarter of the deforming workpiece.

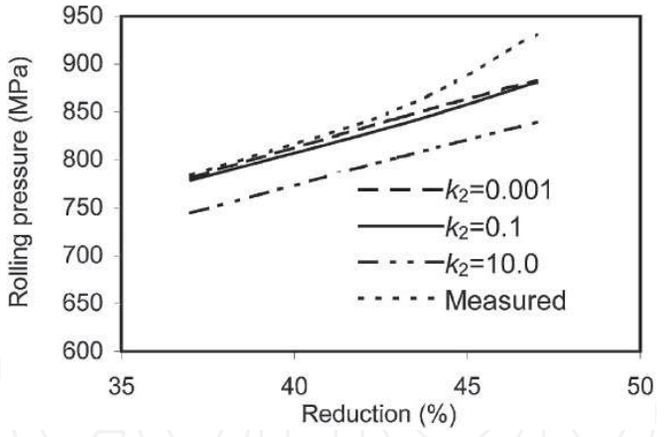

Figure 3. Effect of K_2 on rolling pressure.

and case 2, $K_1 = 0.7$, $K_2 = 1.4$, and $k_1 = k_2 = 0.1$. The friction variation in the roll bite has a significant effect on the spread as shown in **Figure 7**, where the spread calculated through the constant friction model is greater than the result obtained from the friction variation one, and the spread increases with an increase of reduction. The spread decreases when K_1 increases and K_2 decreases (in case 2) due to the increased forward slip as shown in **Figure 8**, more metal flows along the rolling direction, resulting in a decrease of the transverse flow of metal. It is found in **Figure 7** that the effect of friction variation on spread is not significant for reduction < 25%.

http://dx.doi.org/10.5772/intechopen.71880

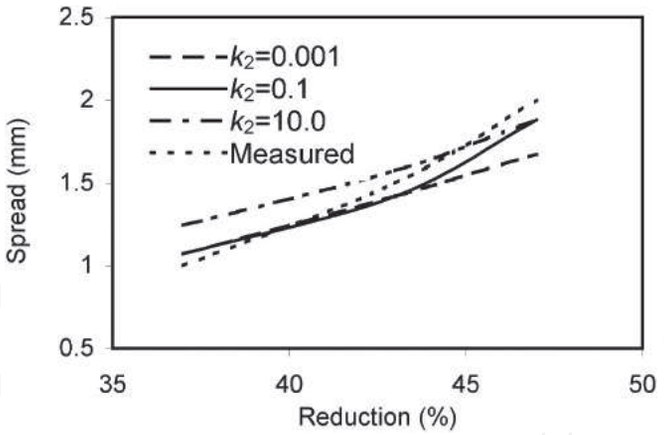

Figure 4. Effect of K_2 on spread.

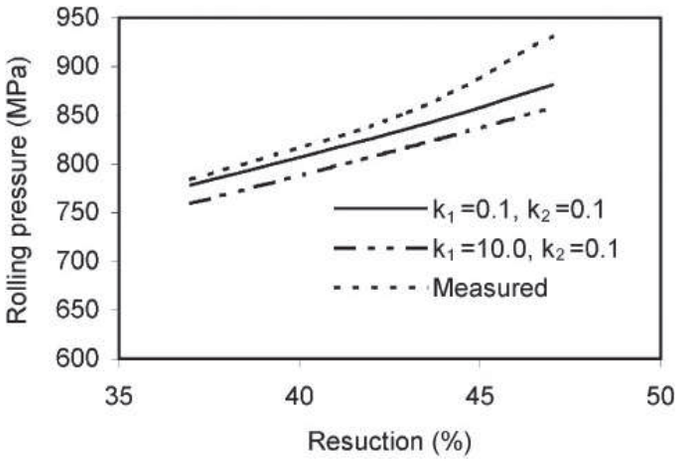

Figure 5. Effect of K_1 on rolling pressure.

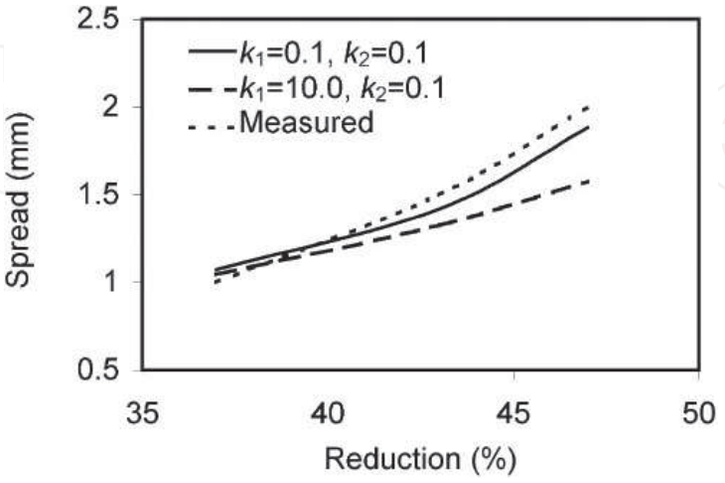

Figure 6. Effect of K_1 on spread.

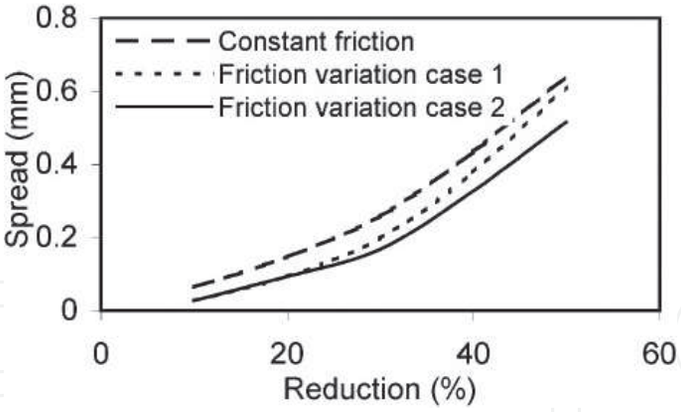

Figure 7. Effect of reduction on spread.

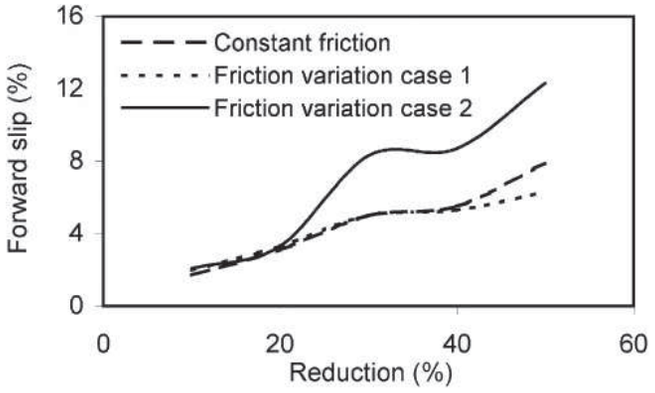

Figure 8. Effect of reduction on forward slip.

3. Application of crystal plasticity finite element method (CPFEM)

Little research has been done on the surface development of constraint surface (surface asperity flattening process) with CPFEM. Most current CPFEM research focus on the development of free surface (surface roughening) by uniaxial and biaxial tensile deformation. In particular, there are almost no reports that mention the relationship between the orientation of surface grains and surface roughness. The texture development of the constraint surface is also a very interesting topic. In metal forming, the strain rate contributes significantly to the workpiece work hardening, but there is little research on how the strain influences the surface roughness. A physical simulation has been conducted on an INSTRON servo-hydraulic testing machine by using a channel die. The relationship between the surface roughness and related parameters such as gauged reduction, friction, texture (grain orientation), and grain size and strain rate has been identified.

The methodology of crystal plasticity finite element modeling (**Figure 9**) follows the rules as: rate-dependent crystal plasticity constitutive models will be written into the UMAT and then used in the ABAQUS main program (geometric model). The geometric model is established based on experimental conditions (reduction, strain rate, friction, original surface roughness, and original texture information). The modeling results will be compared with the

http://dx.doi.org/10.5772/intechopen.71880

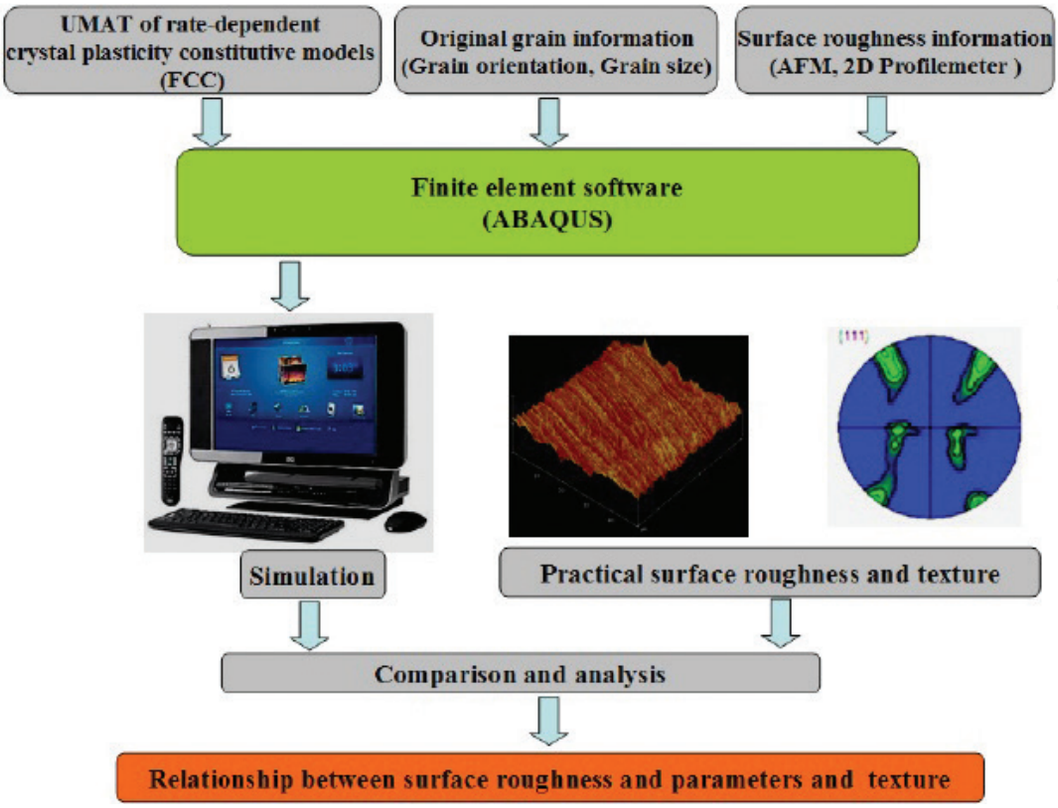

Figure 9. Methodology of crystal plasticity finite element modeling.

experimental results. Furthermore, the relationship between the surface asperity flattening process (surface roughness) and the above-mentioned parameters will be investigated. The mechanism of surface asperity flattening will be analyzed.

Flow rule of plastic deformation gradient F^p can be expressed [7]:

$$\dot{F}^p F^{p^{-1}} = \sum_{\alpha=1}^{n} \gamma_{(\alpha)} \dot{S}_{(\alpha)} \otimes m_{\alpha} \tag{3}$$

where $\dot{\gamma}_{(\alpha)}$ is the plastic shear rate of the αth slip system.

The relationship between the shear rate $\dot{\gamma}_{(\alpha)}$ and the resolving shear stress $\tau_{(\alpha)}$ is formulated below [7]:

$$\dot{\gamma}_{(\alpha)} = \dot{\gamma}_0 \, sgn\,(\tau_{(\alpha)}) \left| \frac{\tau_{(\alpha)}}{S_{(\alpha)}} \right|^{1/m} \tag{4}$$

For cubic metal, the hardening equation of the slip system can be simplified as [7]:

$$\dot{S}_{(\alpha)} = \sum_{\beta=1}^{n} h_{\alpha\beta} \left| \dot{\gamma}_{(\beta)} \right| \tag{5}$$

where $h_{\alpha\beta}$ is the hardening matric of the slip system α led by the slip system β.

3.1. Three-dimensional (3D) model

A three-dimensional model based on crystal plasticity finite element (CPFE) is proposed according to the atomic force microscopy (AFM) experimental values where the results are sorted and applied in MATLAB for modeling the surface morphology. Every four neighboring elements at the top surface have one orientation for keeping the weight function of orientation in the model. Some elements on the top surface are refined. There are 840 C3D8R integration elements; among them 280 elements are with 70 Euler angle triplets and the others are featured by one element with one orientation. Both the tool and mold have 460 discrete rigid elements. A spatial orientation distribution has been assigned for the workpiece based on the electron backscatter diffraction (EBSD) experimental results.

The relationship between the AFM measured results, the MATLAB calculated results, and 3D CPFE model is shown in **Figure 10**. Direction 1 corresponds to the rolling direction, direction 2 to the normal, and direction 3 to the transverse direction. The three-dimensional model is 100 μm × 100 μm × 100 μm in size. Due to the small size of the sample, only a quarter of practical samples were chosen for simulation. It is considered that during the modeling, the combined slip system includes 12 {110} <111> slip systems (slip planes and slip directions). A total of 630 Euler angle triplets from the experimental results were input into ABAQUS as the initial crystallographic condition of the 3D model [7, 8]. All the parameters of simulation are taken from **Table 1** as a reference.

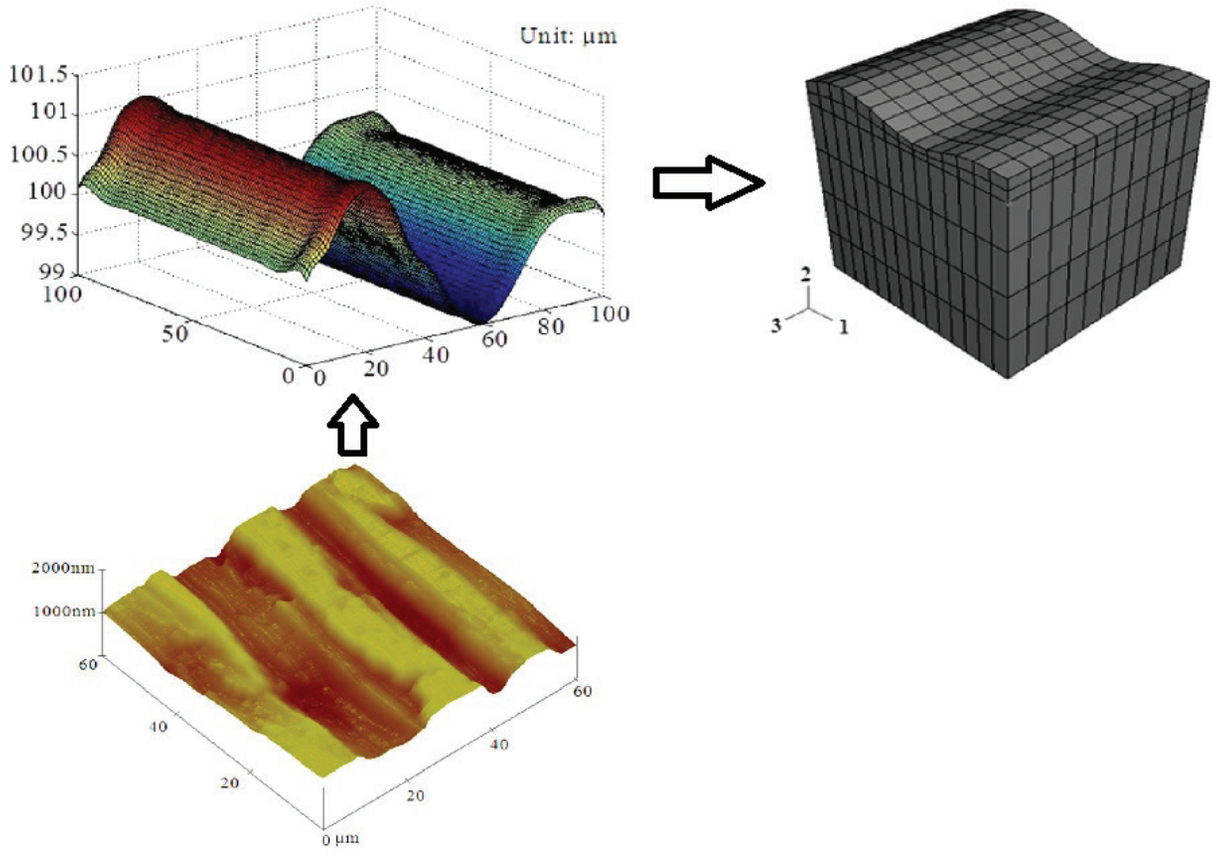

Figure 10. Relationship between AFM, MATLAB, and the 3D CPFE model.

Parameter	Value	Parameter	Value
C_{11}	106,750 MPa	s_0	12.5 MPa
C_{22}	60,410 MPa	h_0	60 MPa
C_{44}	28,340 MPa	s_s	75 MPa
$\dot{\gamma}_0$	0.001	a	2.25
m	0.02	q_1	1.0 (coplanar)
			1.4 (no coplanar)

Table 1. Material parameter of aluminum.

3.2. Results and discussion

3.2.1. Influence on surface roughness

Figure 11 shows that the surface asperity of the samples tends to be flattened with an increase of reduction. With an increase in reduction, the sample with a higher strain rate has a higher flattened rate of surface asperity than the sample with a lower strain rate. Increasing the applied macroscopic strain rate will increase the shear rate of lip systems in the surface area. Then under the same reduction, the sample deformed at a higher strain rate will activate more slip systems in the surface area. When the reduction is 40%, the surface roughness R_a of the sample with a higher strain rate is 0.16 μm, while the sample with a lower strain rate is only 0.09 μm.

3.2.2. Influence of the strain rate on hardness

Figure 12 shows the influence of the strain rate on the hardness of the sample, and the influence is nonlinear. There are different stages in the evolution of hardness because when the

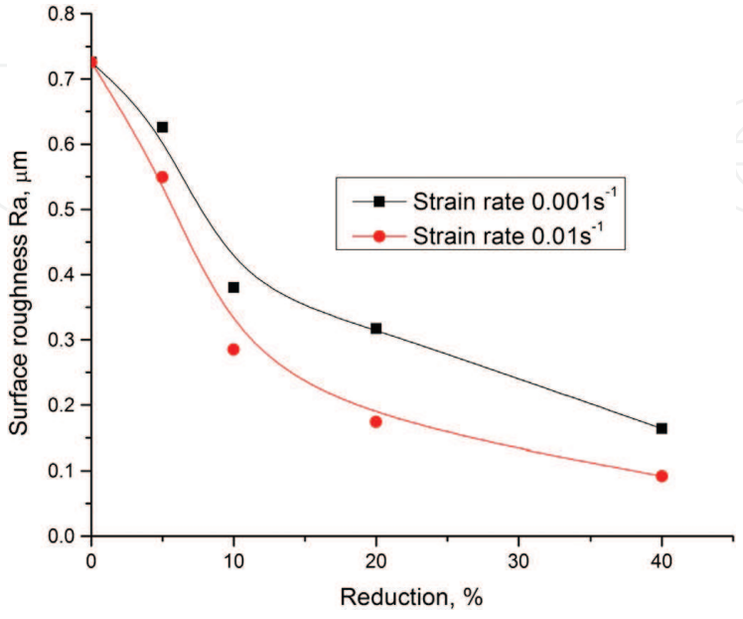

Figure 11. Influence of strain rate on surface roughness.

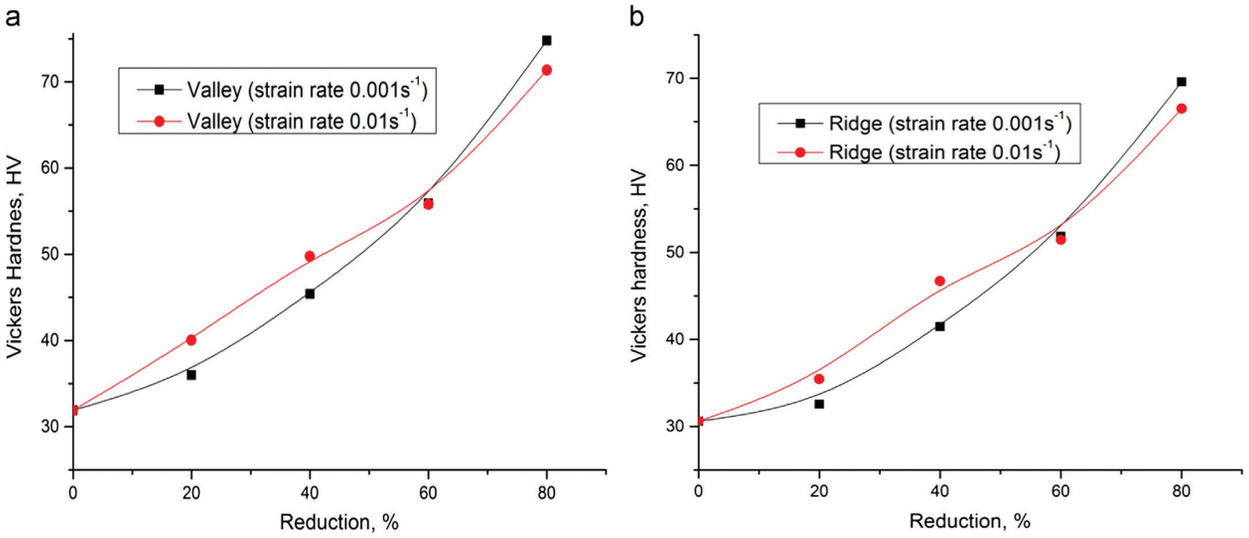

Figure 12. Influence of the strain rate on hardness (a) valley and (b) ridge.

reduction is lower (less than 60%), increasing the strain rate generally increases the hardness. At a larger reduction, increasing the strain rate will decrease the hardness under the same reduction [23]. When the reduction is lower, increasing the strain rate can increase the shearing rate of slip systems and also increase the density of dislocation. However, when reduction exceeds a certain value, the dislocation motion will overcome the barrier of grain boundary. In some areas, the density of dislocation decreases.

3.2.3. Effect of strain on surface roughness (R_a)

In **Figure 13**, both the experimental and simulation results show the same tendency that increasing the strain rate can lead to a decrease in surface roughness under the same reduction. When reduction is less than 10%, the effect of the strain rate on surface roughness is insignificant, where mostly elastic deformation influences the flattening behavior of surface asperity. In this case, the increase of strain rate affects insignificantly the elastic deformation surface roughness. Plastic deformation plays an important role on surface area when the reduction exceeds 10%. When slip is the only deformation mode, the increased strain rate can result in more slip through the increased slip shear rate. Therefore, the surface roughness will decrease greatly with an increase in the strain rate.

3.2.4. Effect of the strain rate on texture

Figure 14 shows that the influence of strain rate on the pole figures with at strain rate of 0.001 s^{-1} and 0.01 s^{-1} is not significant. In this case, every experiment has been carried out at room temperature, and the two applied strain rates are quite small. Deformation under the two strain rates belongs to the quasistatic deformation, and the difference between the two applied strain rates is small compared to the other dynamic deformation.

http://dx.doi.org/10.5772/intechopen.71880

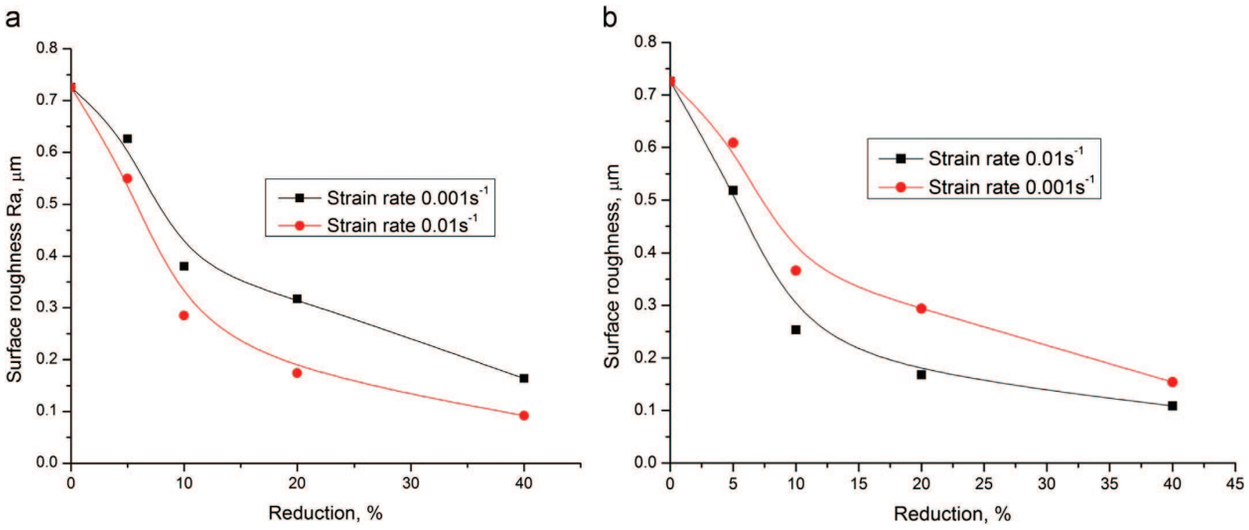

Figure 13. Effect of the strain rate on surface roughness R_a: (a) experimental and (b) simulation.

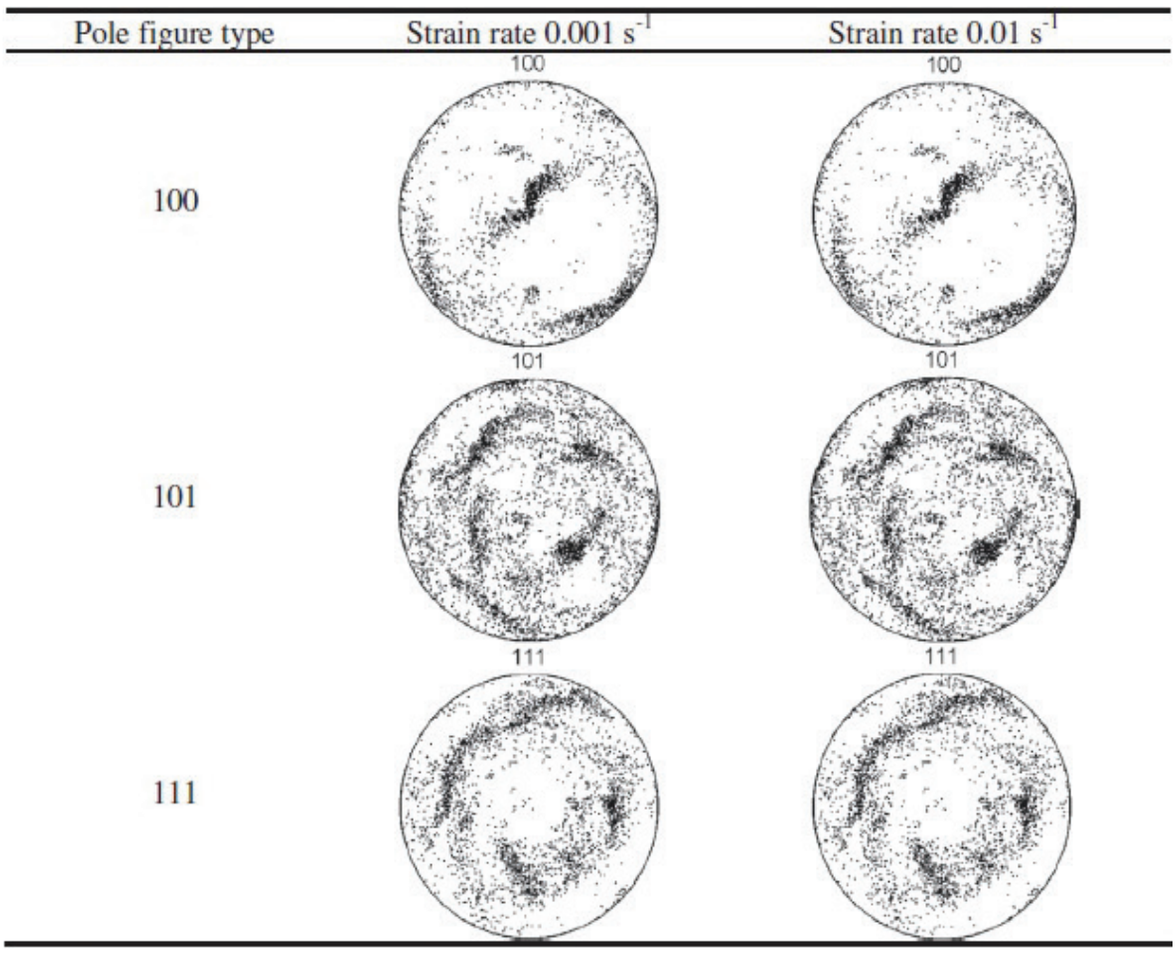

Figure 14. Effect of the strain rate on texture (reduction 60% without lubrication).

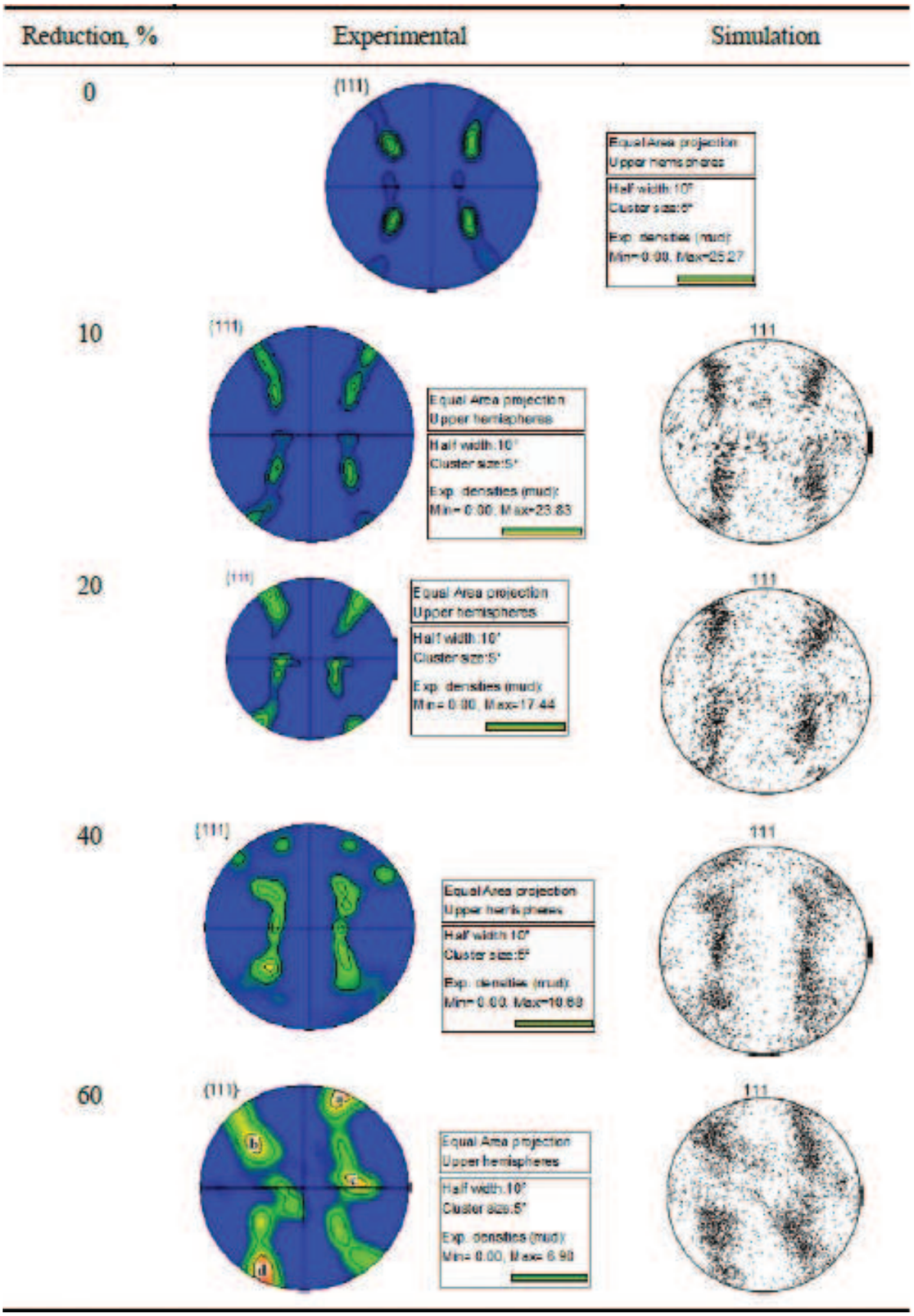

Figure 15. Comparison of the experimental pole figures with the simulation results.

http://dx.doi.org/10.5772/intechopen.71880

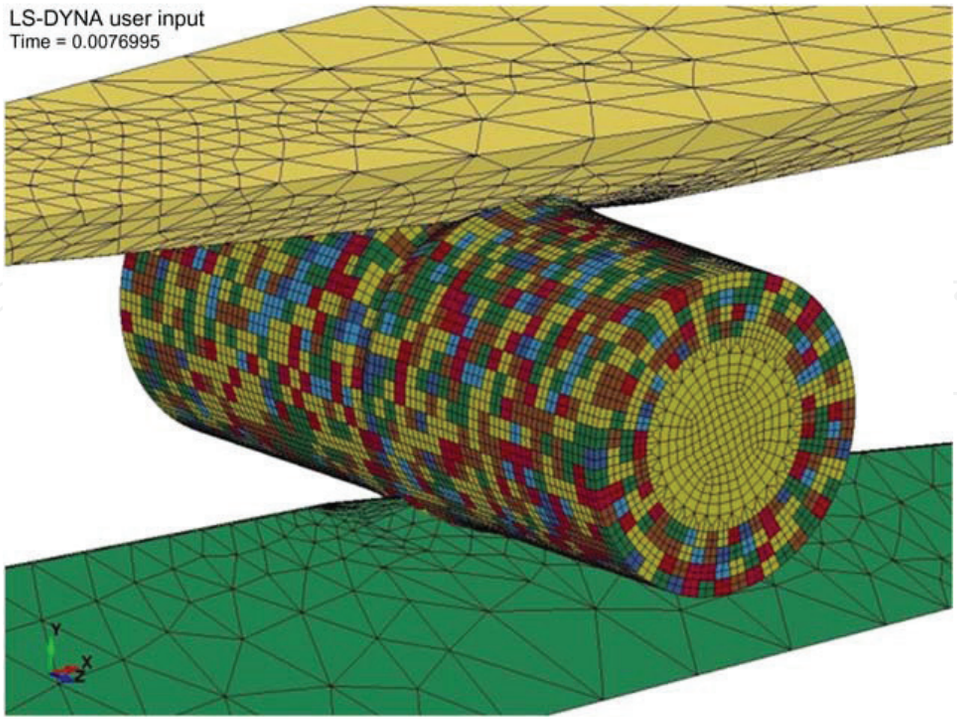

Figure 16. FE model in grained heterogeneities of workpiece in MCWR.

3.2.5. Analysis of pole figure

Normally, the close-packed plane in FCC metal is {111}. In this case, the pole figure {111} is used for the analysis. Before compression, the sample has a cubic texture {111}<001> as shown in **Figure 16**. The predicted result has been compared to the experimental result; both of them show the same texture development. In the pole figure {111}, with an increased reduction, the brass orientation {110}<112> of silk texture becomes obvious while the cubic texture {001}<100> gets weaker. When the reduction reaches 60%, the brass orientation {110}<112> of silk texture shows extreme strong around a and d areas shown in **Figure 15**. Additionally, some S orientations {123}<634> can be seen in b and c areas. These results are basically in the agreement with the Sarma and Dawson's results [7, 8], which show a consistent development in hardness and grain size.

4. Novel material model based on Hall-Petch relationship in microforming

Size effects in microforming cannot be conveyed by the classical theory of continuum plastic mechanics, which is scale-independent. The specimen size effects on the flow stress of poly-crystalline Cu-Al alloy have been investigated, and the fact that the flow stress decreases with the dimensional reduction of specimen has been explained by the proposed affect zone model [24]. A flow stress model, a function of the ratio of the sheet thickness to grain size, has been established based on Hall-Petch relationship, dislocation pile-up theory, and affect zone model [25]. A mixed material model based on modified Hall-Petch relationship, surface

layer model, and grained heterogeneity is proposed, and the 3D aggregate of polycrystalline is represented by a Voronoi tessellation. The effect of grain size on flow stress is an important aspect of polycrystalline metal plastic deformation. The simulation of microforming processes (micro cross wedge rolling (MCWR), micro flexible rolling and micro V-bending) have been conducted with the consideration of size effects from grain size and feature size. The validation of the proposed material model will be conducted by physical experiments through the comparison between experimental results and simulation ones.

Fundamentals have been developed to build up a FE model considering the occurrence of size effects at microscale by using the ANSYS/LS-DYNA program. The newly developed material model is implemented considering grained heterogeneity. As shown in **Figure 16**, two forming tools and a cylindrical workpiece of 0.831.2 mm^2 are meshed in solid element 164 with an 8-noded structure. In order to reduce computational time and ensure stability in large deformation, viscous hourglass control and one-point integration were applied for all elements. For each grain size, 10 different polycrystalline aggregates of workpiece were generated stochastically by the algorithm of 3D Voronoi tessellation. The simulation was performed by applying equal and opposite velocities to forming tools in the horizontal (x) direction. In whole process, the workpiece is left unconstrained, and the tools are held in the vertical (y) direction and in the out-of-plane (z) direction [12]. **Figure 17** shows the process of forging shape during micro cross wedge rolling.

Laminar cricoid distribution of strain is typical in conventional CWR with homogeneous material properties and also exists in MCWR where billet material is homogeneous (**Figure 18a**). However, the grained heterogeneity effects on the metal deformability and strain distribution should be considered in microscale forming. It is shown in **Figure 18b–d** that the continuous laminar distribution of strain in the workpiece has been disturbed due to the inhomogeneous

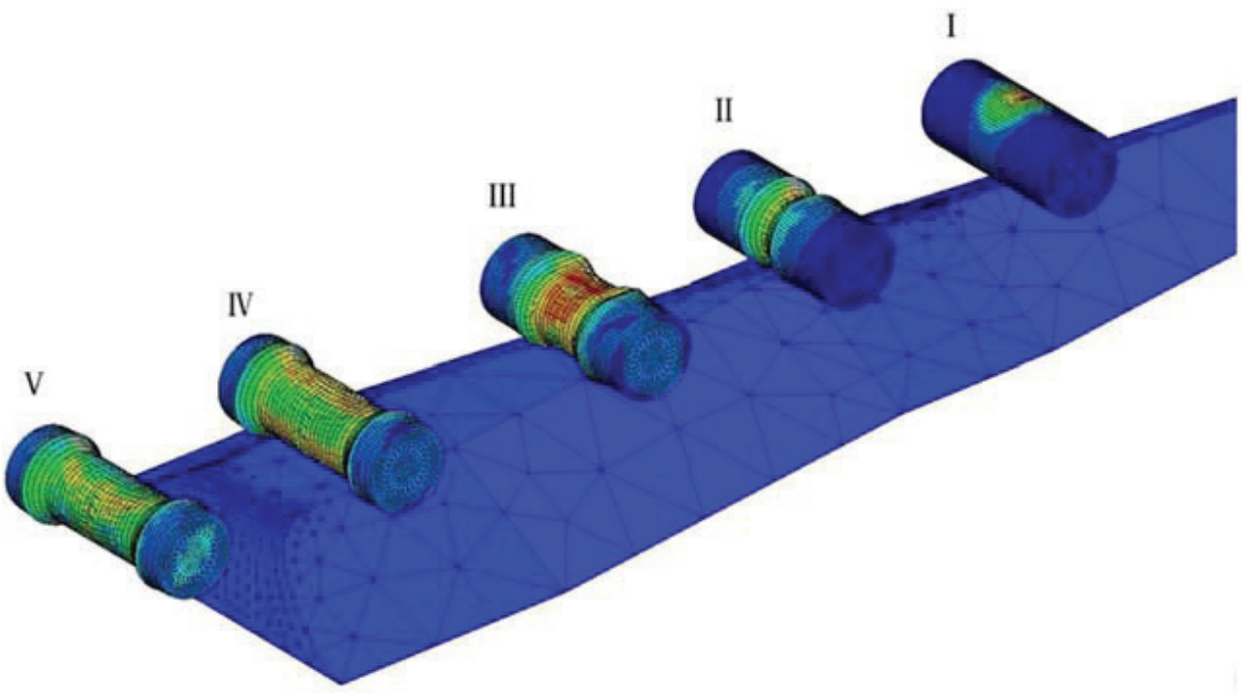

Figure 17. Process of forging shape during MCWR.

http://dx.doi.org/10.5772/intechopen.71880

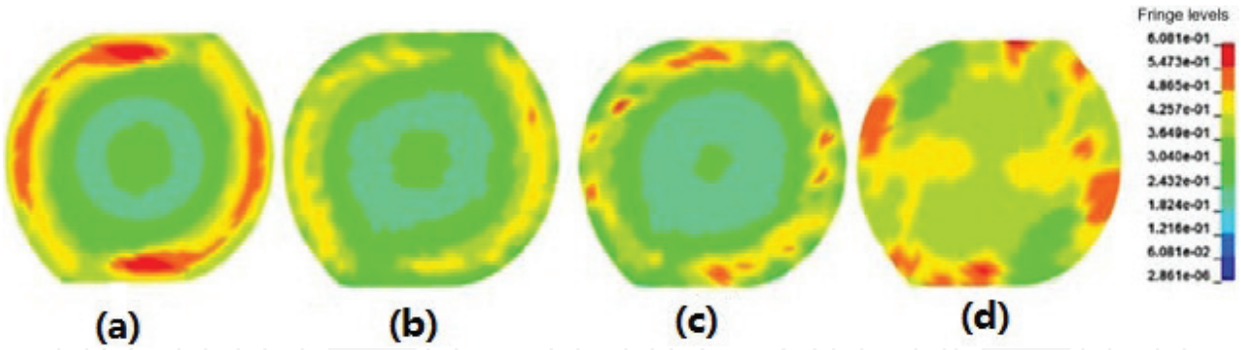

Figure 18. Distribution of effective strain of the medial section in axial direction (a) uniform material properties and (b, c, d) inhomogeneous material properties with grain sizes of 6, 40, and 120 μm, respectively.

mechanical properties [12–14]. The location of the maximum strain and stress cannot be determined easily as that in the conventional CWR process.

The stress and strain distribution on the profile for the halved 250 μm thick workpiece consisting of grains with the average grain size of 250 μm is illustrated in **Figure 19**. The stress-strain distribution is inhomogeneous because only some grains are in plastic regime while others still undergo elastic strain regime during the flexible rolling process [15].

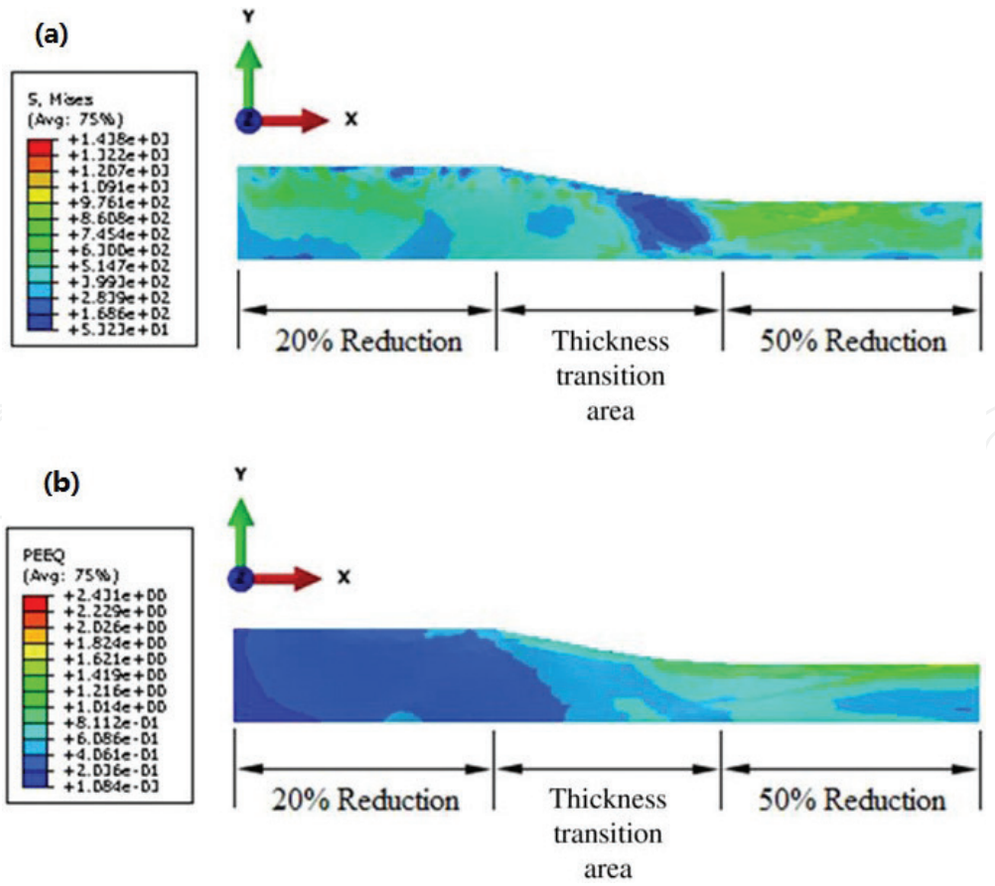

Figure 19. Stress-strain distribution on the profile after springback in micro flexible rolling: (a) von Mises stress distribution and (b) equivalent plastic strain distribution.

Figure 20 shows the tension effect on the average springback from the proposed models. Regardless of the initial thickness and pass reduction, the springback decreases moderately when the front and back tensions increase in increments of 25 MPa from 0 to 100 MPa. For thicker workpiece, front and back tensions have a significant influence on eliminating the springback due to that front and back tensions are able to improve metal flow and relax residual stresses and then increase the thickness precision of rolled workpiece.

In **Figure 21**, it can be seen that the thickness springback increases as the initial workpiece thickness decreases. For a certain grain size, the grain number decreases in thickness direction for less thick workpiece. Therefore, the effect of each single grain plays a very significant role on the springback resulting in larger springback value. For each thickness, the curves are in similar trends under different reductions, and the springback difference is below 10.5% for each grain size, which is close to the simulation result.

Micro V-bending process is simulated with an implicit FEM package: ABAQUS/Standard. The processing parameters in the simulation are the same as those in physical experiments, and the value of coefficient of friction is set to be 0.02. The FE model of micro V-bending with Voronoized specimen is shown in **Figure 22a**. **Figure 22b** illustrates the grain heterogeneity in Voronoized specimen, among which different colors represent different mechanical properties of grains. It is shown in **Figure 23** that the upper bound grain plastic property is illustrated by dark blue (six grains), while light blue (six grains) is for the lower bound grain plastic property [16]. The FE model is close to real physical test condition as the right and the left sides of the sample are not equal in terms of grain size and the scatter of mechanical properties of grains, rather than set up as a traditional asymmetrical one.

Figure 24 shows the simulation result of micro V-bending. The inhomogeneous deformation occurs significantly during bending process. The different colors in middle deformation zone represent that different grains have undergone different deformation because of grain heterogeneity. In the bending process, some grains first reach their yield stress and undergo plastic deformation prior to other grains. Even the workpiece has started the plastic deformation, some grains with higher yield stress may still be under elastic stress condition. This sort of grain heterogeneous deformation could influence the springback significantly and should be taken into account in numerical simulation of microforming [16].

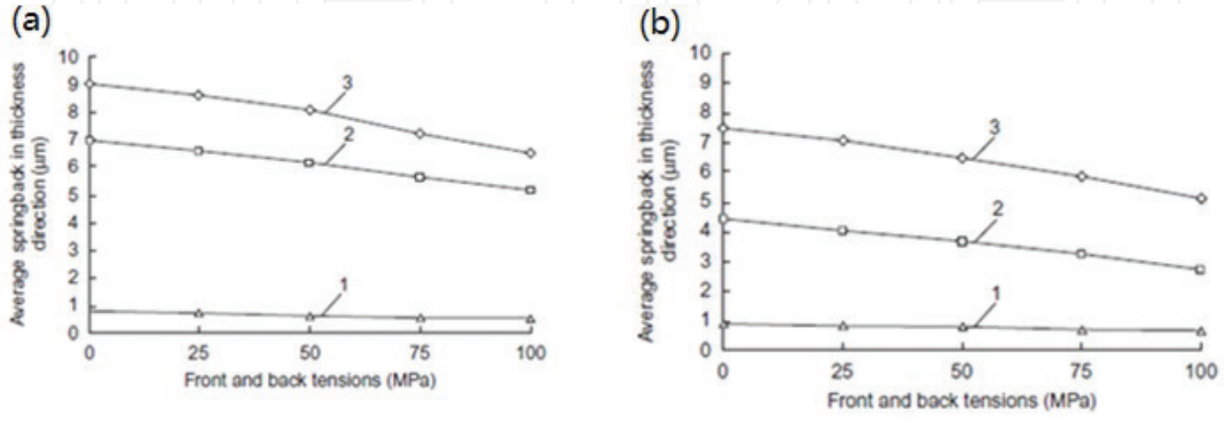

Figure 20. Relationship between average springback in thickness direction and front and back tensions for initial workpiece thickness of 100, 250, and 500 μm: (a) 20% reduction and (b) 50% reduction.

http://dx.doi.org/10.5772/intechopen.71880

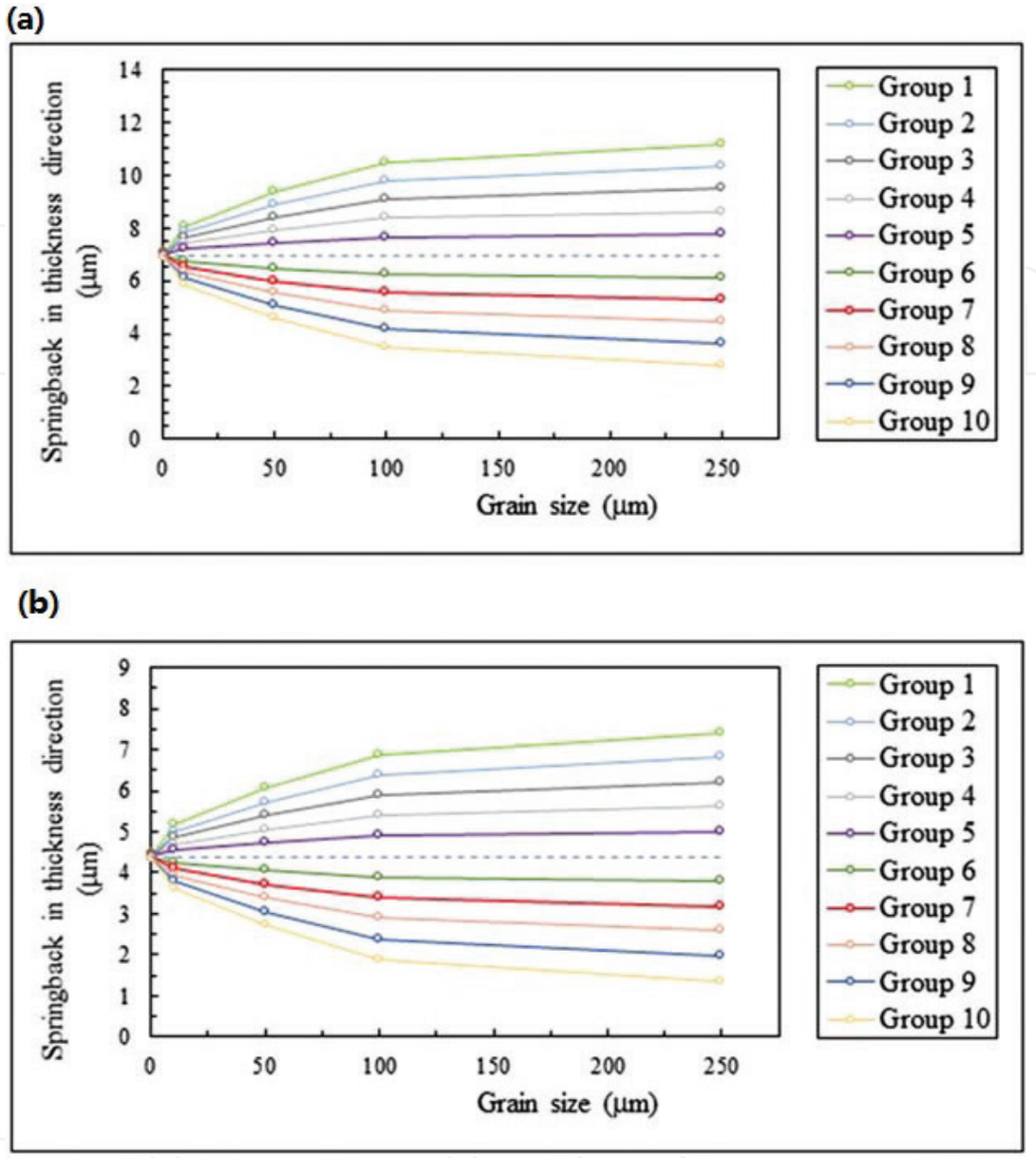

Figure 21. Springback in thickness direction versus gain size for initial workpiece thickness of 100 μm: (a) 20% reduction and (b) 50% reduction.

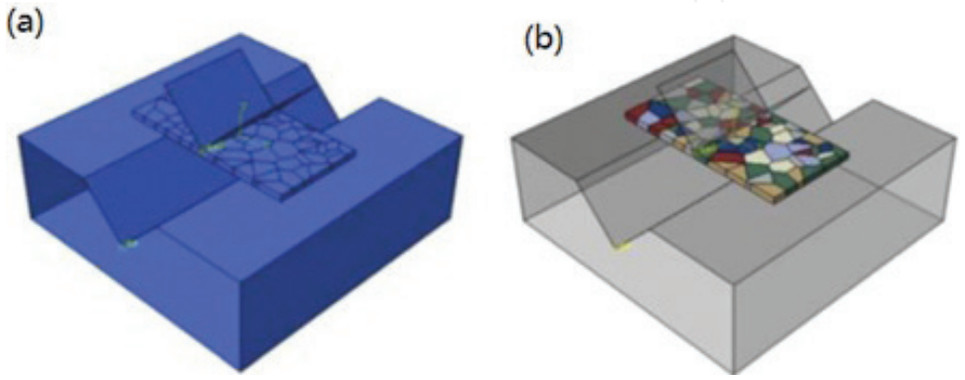

Figure 22. FEM simulation of micro V-bending with (a) Voronoi tessellations and (b) grain heterogeneity.

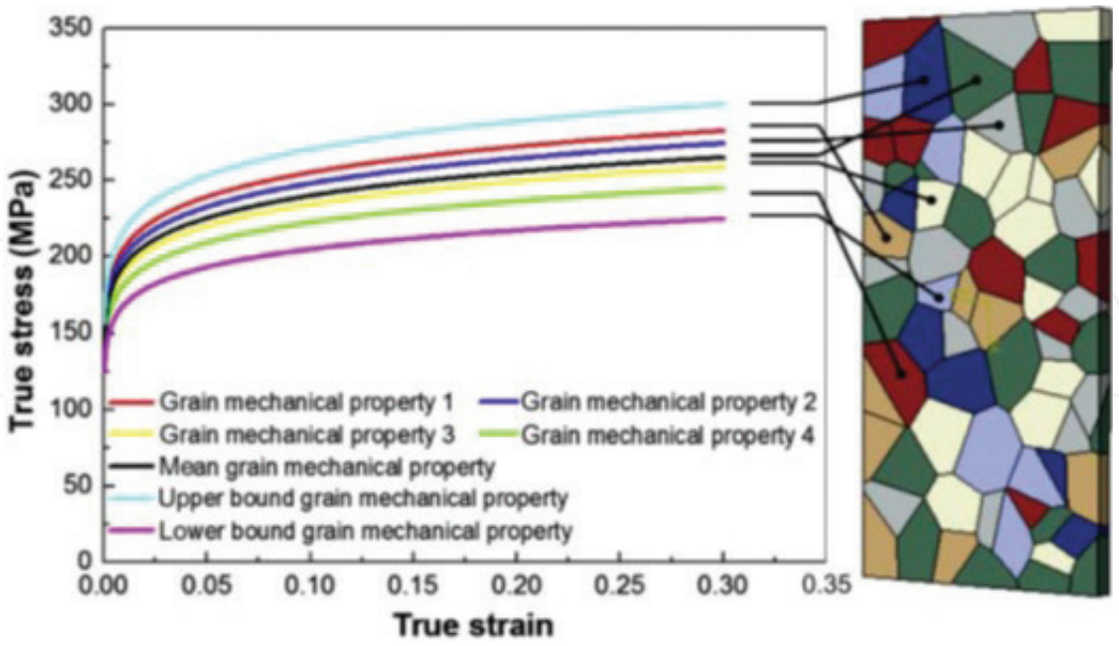

Figure 23. Grain properties randomly assigned on a Voronoized bending sample.

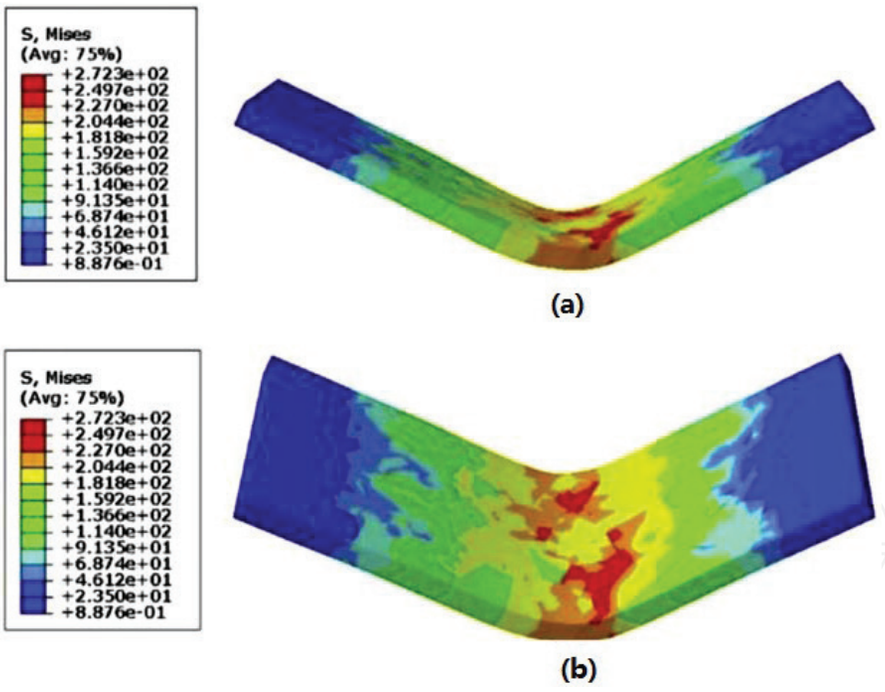

Figure 24. (a) Final angle after springback and (b) von Mises stress distribution.

Seven plastic properties are obtained by experiment and calculation, and they are randomly distributed in bending specimens. Specimens with different random grain heterogeneity distributions are exhibited in **Figure 25**, which are called models "1," "2," "3," "4," "5," "6," and "7," respectively. Seven groups of micro V-bending FE simulations have been conducted with above-mentioned seven specimens individually. Springback angles of seven simulations and an average value are measured and calculated, as shown in **Table 2**.

http://dx.doi.org/10.5772/intechopen.71880

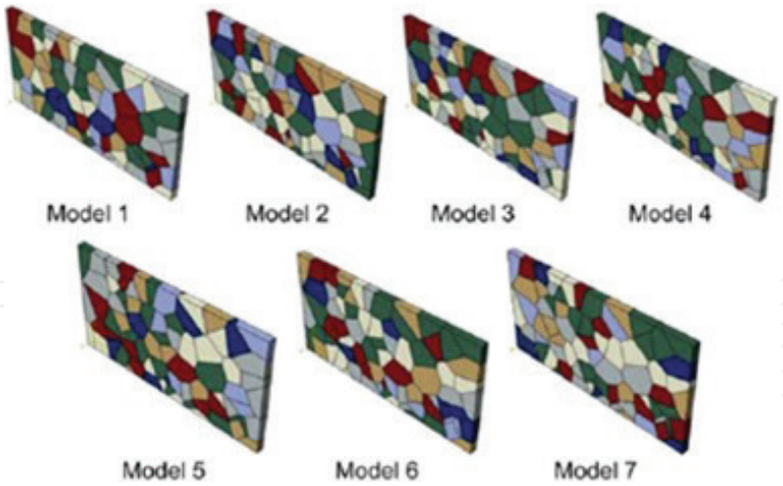

Figure 25. Bending specimens with different gain heterogeneity distributions.

Distribution group	1	2	3	4	5	6	7	Average
Springback angle	30.52	27.37	32.09	31.78	33.44	28.65	34.12	31.14

Table 2. Springback angles from FE simulation (degree).

5. Modified FEM with the consideration of material and lubrication characterization in MDD and MHDD

Figure 26 represents a typical EBSD microstructure. First, the EBSD image was input into the MATLAB software, and the binary image was obtained with black grain boundaries and white grains. Noise and small holes were eliminated in the transformation. Then, the Moore-Neighbor tracing algorithm modified by Jacob's stopping criteria was applied in the binary image treatment. As shown in **Figure 26b**, the information of grains and individual closed subareas, including single grain's area, geometrical center and geometrical orientation, was detected and sorted in MATLAB. The blue ports in **Figure 26b** are the grain's geometrical centers [9, 20, 21].

Figure 27 displays the Voronoi structures and their corresponding FE models with average grain sizes of 10, 20, and 40 μm, respectively.

After annealed at 1100°C, the 50 μm thick blanks, with equiaxed crystals microstructure and average grain size of 40 μm, were drawn into micro cups. The drawn cup mouth is shown in **Figure 28a**, and the maximum thickness distributions of drawn cups are illustrated in **Figure 28b–d**, which represented the new developed model, a Voronoi model without the consideration of grain boundaries and a normal model in homogeneous material properties, respectively. The comparison of the maximum wall thickness between the simulation and the experimental results has been conducted. The localized deformation is ignored, and the maximum thickness was averaged with the lowest peak thickness values for all the simulation cases. It can be seen that the new model and the Voronoi model considered microscopic heterogeneity have higher maximum thickness than that in the normal model [9], where the largest thickness is obtained from the Voronoi model without grain boundaries buffer.

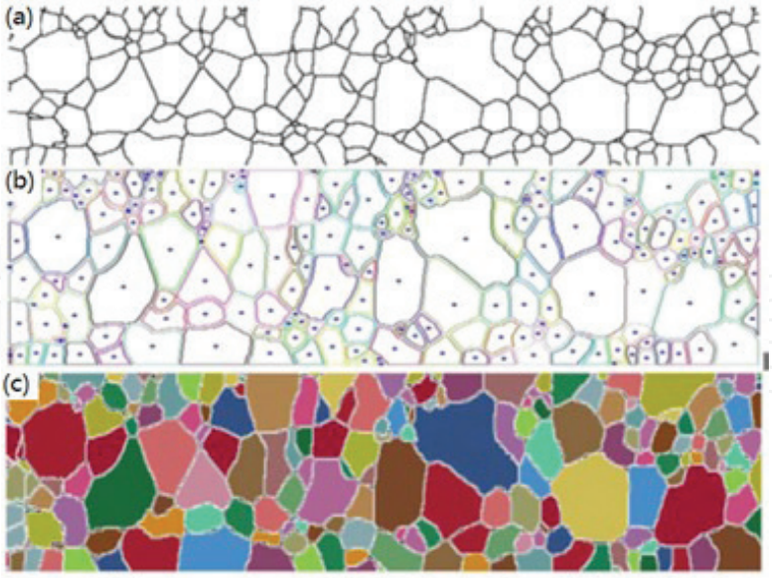

Figure 26. (a) Microstructure of a sample from EBSD, (b) its corresponding geometry detected by MATLAB and (c) corresponding simulation model.

The material surface consists of lots of peaks and valleys called roughness in microforming. The roughness and the extent of the valleys get larger compared to the scaled down workpiece size. As shown in **Figure 29**, the lubricant cannot be retained in the valleys connected to the edge of the blank, and this area is called open lubricant pockets (OLPs) [9, 18, 19]. The fraction of OLPs increases with the decrease in specimen size. The friction force increases because the lubricant cannot be kept during microscale forming process. Therefore, the OLPs must be taken into account when studying the tribological behavior of microforming.

Figure 30 shows schematic of evaluation test for OLPs utilizing liquid where the blank is compressed by the tools under approximately 20 MPa contact pressure. During experiment, the liquid is filled into the tool first, and the liquid intruded area is colored. Then the blank

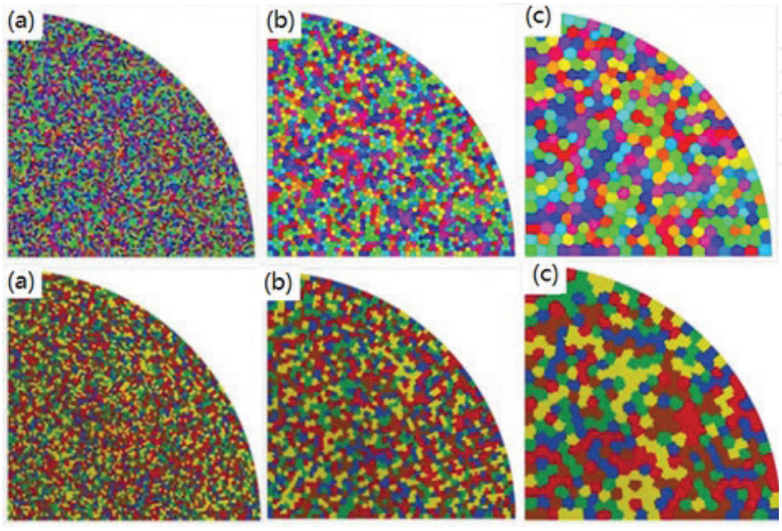

Figure 27. Voronoi structures (in the first line) and their corresponding FE models (in the second line): average grain sizes of (a) 10, (b) 20, and (c) 40 μm.

http://dx.doi.org/10.5772/intechopen.71880

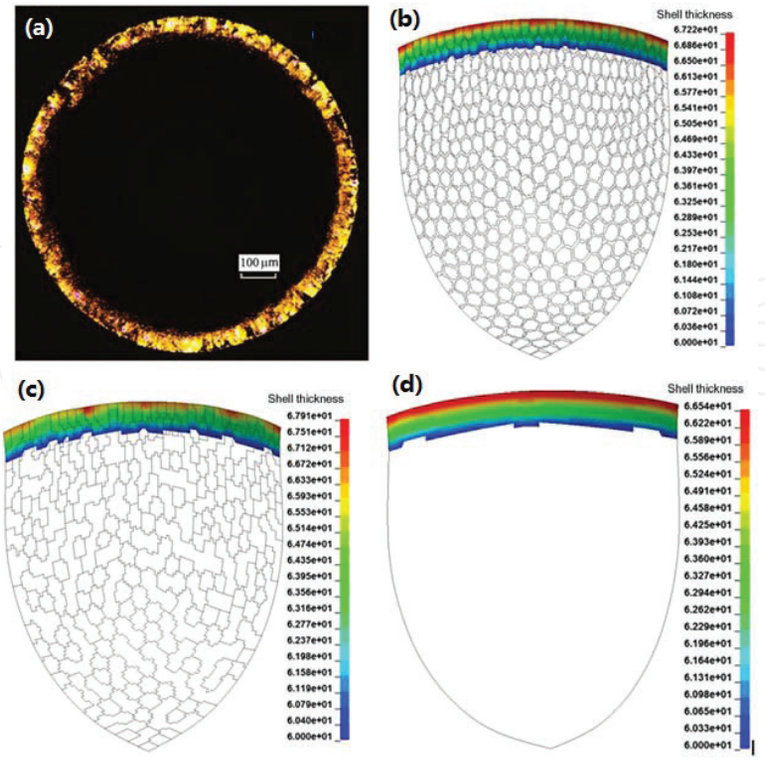

Figure 28. (a) Drawn cup with 1100°C annealed blank and maximum thickness distribution from the simulation with (b) the developed new model, (c) the Voronoi model, and (d) the normal model.

with visualized, and liquid intruded area is taken out when the liquid dries out. After this, the blank surface is observed under a digital microscope, and the pictures are digitized [9, 17].

Figure 31 illustrates the effects of scale factor on the normalized punch force-stroke curves at MDD with lubrication and MHDD with radial pressure. The shape of punch force-stroke curves in λ = 1, 2 is as similar as that with λ = 50 at MDD and MHDD. In these conditions, only the inner or outer pockets exist in the flange area. Therefore, the coefficient of friction in the flange area is almost uniform. On the other hand, in λ = 5, the inner and outer pockets are

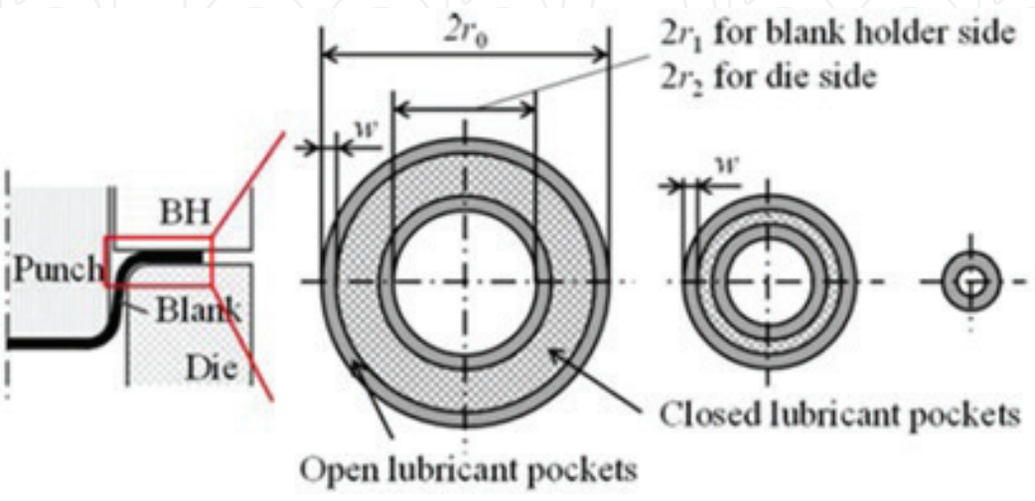

Figure 29. The change of fraction of OLPs in flange area with the decrease of blank size.

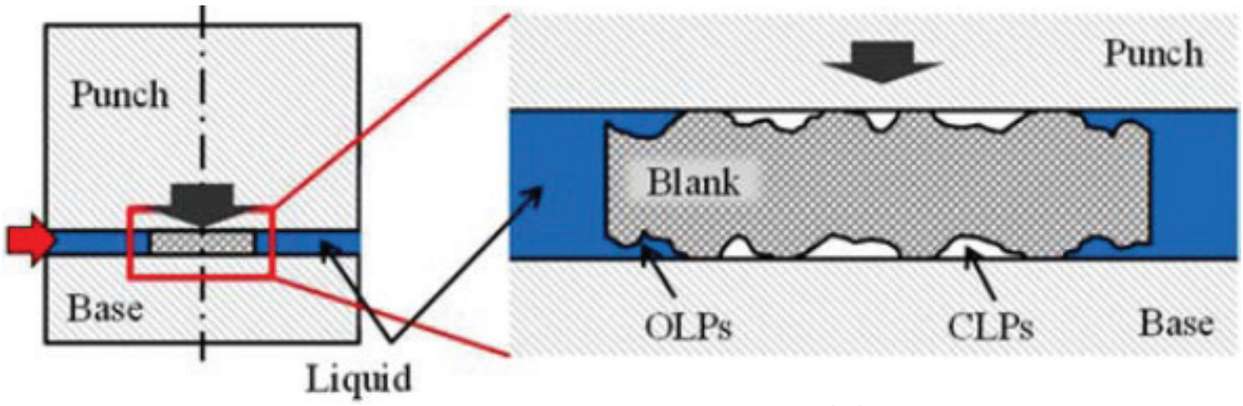

Figure 30. Schematic of evaluation test for OLPs utilizing liquid.

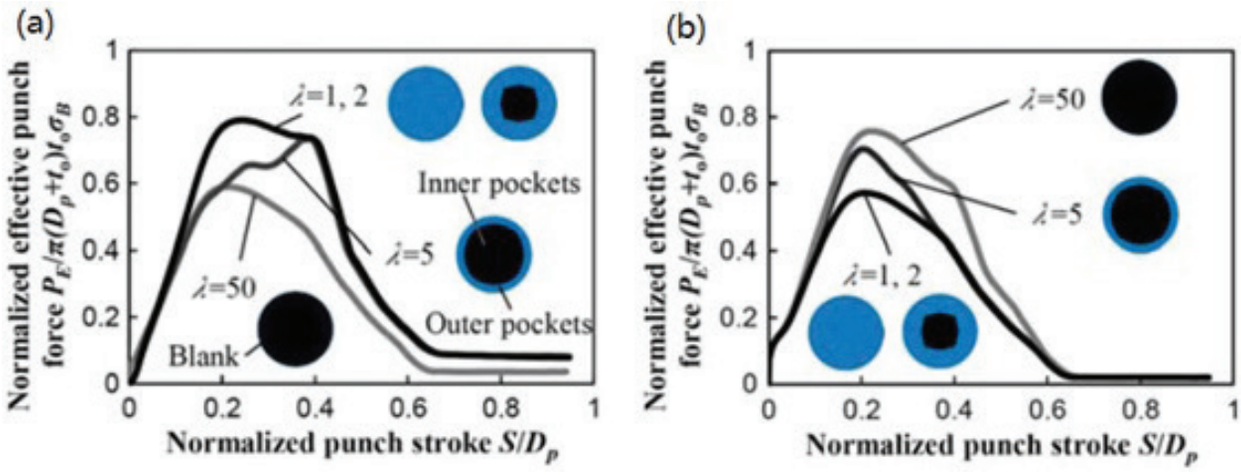

Figure 31. Effects of scale factor λ on normalized punch force-stroke curve at different lubrication conditions (a) MDD with lubrication, and (b) MHDD with radial pressure.

mixed in the flange area. In the initial process, the inner pockets mainly exist at die shoulder and flange area and affect the tribological behavior significantly. Therefore, the punch force-stroke curves are as similar with that in macroscale. However, in the middle process, the ratio of outer pockets increases. As a result, the tribological behavior shifts to that in microscale. This behavior appears at both MDD and MHDD. This causes the maximum punch force shifts as shown in **Figure 31a**. These results indicate the ratio of the outer pockets to the flange area during the forming process influences the tribological behavior of the MHDD as shown in **Figure 31b**.

Figure 32a shows the tribological size effects in MDD and MHDD. With the decrease in the size, the friction force increases in case of MDD with lubrication because the ratio of outer pockets increases. When λ = 1, 2, the maximum effective punch forces in MDD with the dry friction and lubrication become the same because only the outer pockets exist at flange area. On the other hand, with the decrease in the size, the friction force in MHDD decreases. It can be seen the tribological size effects in MHDD have an opposite behavior with MDD. In MHDD, the fluid medium is provided to the outer pockets whose ratio is high in microscale. This

http://dx.doi.org/10.5772/intechopen.71880

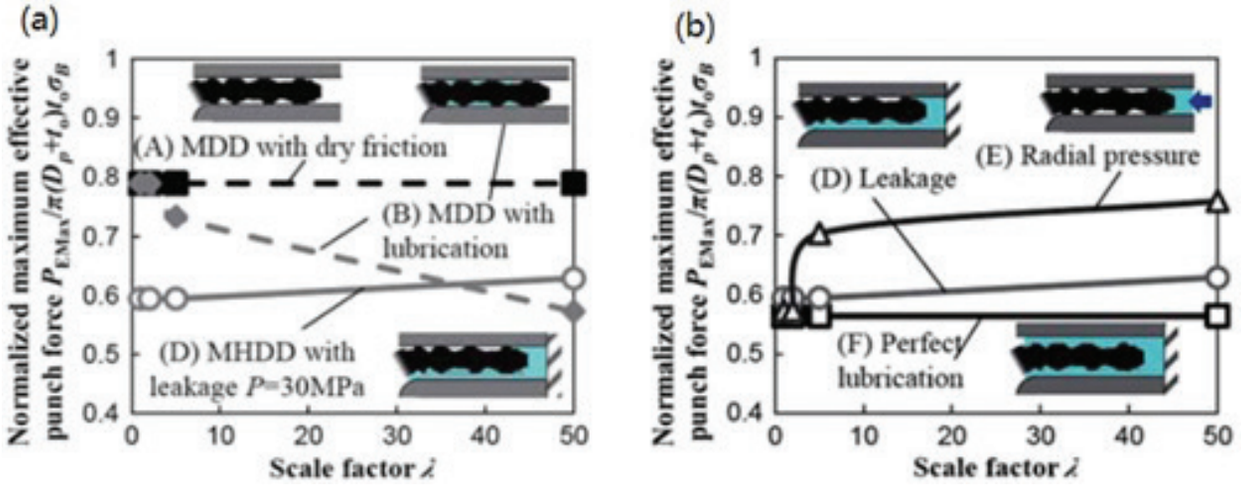

Figure 32. Tribological size effects at different lubrication conditions in MDD and MHDD.

caused the decrease in friction force in MHDD. **Figure 32b** shows the effect of the lubrication type on friction force in MHDD. The decrease of friction force in radial pressure condition is much larger than that in leakage condition. Also in radial pressure condition, the friction force significant decreases from $\lambda = 5–1$. It is because the contact pressure between the blank and die at die shoulder is higher than that between the blank and blank holder in the small D_p/t. Therefore, the decrease in coefficient of friction at die shoulder is especially important to decrease the friction force in MHDD. According to the above-mentioned results, the friction force can decrease with the decrease in size in MHDD, while it only increases in MDD. The friction force can be reduced by filling the fluid medium in the outer pockets in MHDD [19].

6. Conclusions

This chapter presents the applications of FEM in metal-forming analysis from macroscale to microscale, including FEA software programs used, simulation approach and results obtained, and their validation for metal-forming processes. A 3D rigid plastic FEM is used with the consideration of friction variation models in the case of work roll kiss occurrence during cold rolling of thin strip. The modeling of the friction variation can produce a more accurate model that can improve the accuracy of simulation results. In the CPFEM, the simulation results show that with an increase in reduction, the cubic texture {001}<100> is weak, while the brass orientation {110}<112> becomes strong. The simulation result agrees with the experimental one. When reduction exceeds 60%, most grains have plastic slips. With an increase in reduction, both the grain size and surface roughness decrease while the flow stress increases. Novel material model with grained heterogeneity in 3D Voronoi tessellation has been developed in the simulation of micro cross wedge rolling, springback analysis in thickness direction during micro flexible rolling process and the micro V-bending process considering grain boundary and generation process of grains in the workpiece. Real microstructures and Voronoi structures are applied in microstructural models through image-based modeling method and

modified FE with the consideration of size effects including material characterization, friction/contact characterization, and other size-related factors. Open and closed lubricate pocket theory and size-dependent coefficient of friction are also proposed in micro deep drawing and micro hydromechanical deep drawing.

Author details

Zhengyi Jiang* and Haibo Xie

*Address all correspondence to: jiang@uow.edu.au

School of Mechanical, Materials, Mechatronic and Biomedical Engineering, University of Wollongong, Wollongong, NSW, Australia

References

[1] Liu Y, Tieu A, Wang D, Yuen W. Friction measurement in cold rolling. Journal of Materials Processing Technology. 2001;**111**:142-145. DOI: 10.1016/S0924-0136(01)00541-6

[2] Zhang L. On the mechanics of cold rolling thin foil. International Journal of Machine Tools and Manufacture. 1995;**35**:363-372. DOI: 10.1016/0890-6955(94)E0028-H

[3] Fleck N, Johnson K, Mear M, Zhang L. Cold rolling of foil. Proceedings of the Institution of Mechanical Engineers, Part B: Journal of Engineering Manufacture. 1992;**206**:119

[4] Jiang Z, Tieu A. Modelling of rolling of strips with longitudinal ribs by 3-D rigid visco-plastic finite element method. ISIJ International. 2000;**40**:373-379. DOI: 10.2355/isijinternational.40.373

[5] Jiang Z, Tieu A. A 3-D finite element method analysis of cold rolling of thin strip with friction variation. Tribology International. 2004;**37**:185-191. DOI: 10.1016/S0301-679X(03)00049-5

[6] Jiang Z, Tieu A. A method to analyse the rolling of strip with ribs by 3-D rigid visco-plastic finite element method. Journal of Materials Processing Technology. 2001;**117**:146-152. DOI: 10.1016/S0924-0136(01)01087-1

[7] Li H. A Study of Surface Roughness in the Metal Forming Process [Thesis]. Australia: University of Wollongong; 2012

[8] Li H, Öchsner A, Wei D, Ni G, Jiang Z. Crystal plasticity finite element modelling of the effect of friction on surface asperity flattening in cold uniaxial planar compression. Applied Surface Science. 2015;**359**:236-244. DOI: 10.1016/j.apsusc.2015.10.043

[9] Jiang Z, Zhao J, Xie H. Microforming Technology: Theory, Simulation and Practice. Elsevier; 2017. 452 p. ISBN: 9780128112120

[10] Vollertsen F, Hu Z. Tribological size effects in sheet metal forming measured by a strip drawing test. CIRP Annals. 2006;**55**:291-294. DOI: 10.1016/S0007-8506(07)60419-3

[11] Chan W, Fu M, Lu J, Liu J. Modelling of grain size effect on micro deformation behavior in micro-forming of pure copper. Materials Science and Engineering A. 2010;**527**:6638-6648. DOI: /10.1016/j.msea.2010.07.009

[12] Lu H. A Study on the Micro Cross Wedge Rolling of Metals [Thesis]. Australia: University of Wollongong; 2013

[13] Jiang Z, Lu H, Wei D, Linghu K, Zhao X, Zhang X. Finite element method analysis of micro cross wedge rolling of metals. Procedia Engineering. 2014;**81**:2463-2468. DOI: 10.1016/j.proeng.2014.10.351

[14] Lu H, Wei D, Jiang Z, Wu D, Zhao X. Study on the influence of temperature on the surface asperity in micro cross wedge rolling. AIP Publishing. 2013:1032-1037

[15] Qu F, Jiang Z, Lu H. Analysis of micro flexible rolling with consideration of material heterogeneity. International Journal of Mechanical Sciences. 2016;**105**:182-190. DOI: 10.1016/j.ijmecsci.2015.11.004

[16] Fang Z, Jiang Z, Wei D, Liu X. Study on springback in micro V-bending with consideration of grain heterogeneity. International Journal of Advanced Manufacturing Technology. 2015;**78**:1075-1085. DOI: 10.1007/s00170-014-6697-3

[17] Sato H, Manabe K, Wei D, Jiang Z. Numerical modeling of size effect in micro hydromechanical deep drawing. AIP Conference Proceedings. 2013;**1567**:926 http://dx.doi.org/10.1063/1.4850121

[18] Sato H, Manabe K, Ito K, Wei DB, Jiang ZY. Development of servo-type micro-hydromechanical deep-drawing apparatus and micro deep-drawing experiments of circular cups. Journal of Materials Processing Technology. 2015;**224**:233-239. DOI: 10.1016/j.jmatprotec.2015.05.014

[19] Sato H, Manabe K, Wei D, Jiang Z, Alexandrov S. Tribological behaviour in micro-sheet hydroforming. Tribology International. 2016;**97**:302-312. DOI: 10.1016/j.triboint.2016.01.041

[20] Luo L, Jiang Z, Wei D, Manabe K, He X, Li P. An experimental and numerical study of micro deep drawing of SUS304 circular cups. Manufacturing Review. 2015;**2**:27. DOI: 10.1051/mfreview/2015029

[21] Luo L, Jiang Z, Wei D, Manabe K, Zhao X, Wu D. Effects of surface roughness on micro deep drawing of circular cups with consideration of size effects. Finite Elements in Analysis and Design. 2016;**111**:46-55. DOI: 10.1016/j.finel.2015.11.005

[22] Jiang Z, Tieu A. Modelling of thin strip cold rolling with friction variation by a 3-D finite element method. JSME International Journal, Series A. 2003;**46**(3):218-223

[23] Li H, Jiang Z, Wei D, Zhang X. Microtexture based analysis of surface asperity flattening behavior of annealed aluminum alloy in uniaxial planar compression. Tribology International. 2013;**66**:282-288. DOI: 10.1016/j.triboint.2013.04.011

[24] Miyazaki S, Shibata K, Fujita H. Effect of specimen thickness on mechanical properties of polycrystalline aggregates with various grain sizes. Acta Metallurgica. 1979;**27**:855-862. DOI: 10.1016/0001-6160(79)90120-2

[25] Leu D. Modelling of size effect on tensile flow stress of sheet metal in microforming. ASME Journal of Manufacturing Science and Engineering. 2009;**131**:0110021-0110028. DOI: 10.1115/1.3039520